

ULRR

Signal-induced birefringence and dichroism in a tensile-strained bulk semiconductor optical amplifier and its application to wavelength conversion

Item Type	Article
Authors	Guo, Li-Qiang;Connelly, Michael J.
Citation	Journal of Lightwave Technology;23/ 12/ 4037-4045
Publisher	IEEE Computer Society
Download date	2026-05-16 17:01:44
Item License	https://creativecommons.org/licenses/by-nc-sa/1.0/
Link to Item	https://hdl.handle.net/10344/1191

Signal-Induced Birefringence and Dichroism in a Tensile-Strained Bulk Semiconductor Optical Amplifier and Its Application to Wavelength Conversion

Li-Qiang Guo and Michael J. Connelly, *Member, IEEE*

Abstract—Signal-induced birefringence and dichroism in a tensile-strained bulk semiconductor optical amplifier (SOA) are demonstrated in a counterpropagation scheme. The polarization azimuth rotation and the change of ellipticity angle of the probe light are presented on the Poincaré sphere and can be calculated by the Stokes parameters. All-optical wavelength conversion (inverted/noninverted and upconversion/downconversion) based on cross polarization modulation (XPolM) in SOAs are investigated. It is shown that a bit error rate (BER) of $< 10^{-9}$ can be achieved and an extinction ratio of > 9 dB can be obtained at a bit rate of 2.488 Gb/s with a $2^{31} - 1$ non-return-to-zero (NRZ) pseudorandom bit sequence (PRBS). Because of the larger birefringence effect induced by the pump light in the longer wavelength range, upconversion shows better performance than downconversion. Compared with the noninverted case, inverted wavelength conversion shows better performance due to the positive contribution from cross gain modulation (XGM), which takes place simultaneously with XPolM.

Index Terms—Birefringence, cross polarization modulation, dichroism, semiconductor optical amplifier, wavelength conversion.

I. INTRODUCTION

ALL-OPTICAL wavelength converters are the key elements in future wavelength-division-multiplexing (WDM) systems as they can reduce wavelength blocking, provide more flexibility in network management, and offer the possibility of data regeneration [1]. Wavelength converters based on nonlinearities in semiconductor optical amplifiers (SOAs) have been widely investigated in the past few years [2], [3]. Wavelength conversion by cross gain modulation (XGM) in a single SOA has the advantage of simple structure and high conversion efficiency. However, this approach suffers from serious pattern dependence at high bit rate, strong positive chirping (blue shift at rising edge and red shift at falling edge of the pulse), and a degradation of the extinction ratio [4]. Interferometric wavelength converters based on cross-phase modulation (XPM) can realize inverted and noninverted wavelength conversion and offer an improved extinction ratio.

Manuscript received November 8, 2004; revised July 14, 2005. This work was supported by Science Foundation Ireland Investigator Grant 02/IN1/142.

The authors are with the Optical Communications Research Group, Department of Electronic and Computer Engineering, University of Limerick, Limerick, Ireland (e-mail: Li-Qiang.Guo@ul.ie).

Digital Object Identifier 10.1109/JLT.2005.858214

Usually, this approach needs two SOAs integrated on a single chip, which makes it more difficult to control the interferometric arrangement (e.g., Mach-Zehnder) [1], [5]. Wavelength conversion utilizing four-wave mixing (FWM) offers strict transparency, including modulation-format and bit-rate transparency, and is capable of multiwavelength conversions. However, it has low conversion efficiency and needs careful control of the polarization of the input lights [5]. A promising approach to wavelength conversion, which is based on cross polarization modulation (XPolM) utilizing signal-induced anisotropy of nonlinear refraction and absorption in SOAs, has attracted particular interest recently, although the operation had already been demonstrated [6], [7]. This approach utilizes the optically induced birefringence and dichroism in an SOA and has great potential to offer wavelength conversions with high extinction ratios.

In this work, we experimentally present signal-induced birefringence and dichroism in an InGaAsP/InP tensile-strained bulk SOA and then investigate all-optical wavelength conversion based on XPolM. Inverted/noninverted and up/down wavelength conversions are demonstrated at a bit rate of 2.488 Gb/s. Inverted wavelength conversion shows better performance, since XGM, which takes place simultaneously with XPolM, enlarges the effect of inverted wavelength conversion but reduces the effect on noninverted case. Because larger birefringence induced by the pump light in the longer wavelength range overcomes the asymmetrical gain suppression in the SOA and dominates the wavelength conversion operation, upconversion shows better performance than downconversion.

The paper is organized as follows: Section II is devoted to the optically induced anisotropy of bulk SOA; Section III explores the theoretical background of wavelength conversion by XPolM; Section IV presents the experimental methods and results; a few discussions are made in Section V; while in Section VI, some conclusions are drawn.

II. OPTICAL ANISOTROPY OF SOA

A. Strain-Induced Birefringence

The performances of ultrafast nonlinear-optical devices are often determined by the properties of the third-order susceptibility tensor $\chi^{(3)}$ of the nonlinear medium. Cubic materials have three equivalent orthogonal principal axes and are

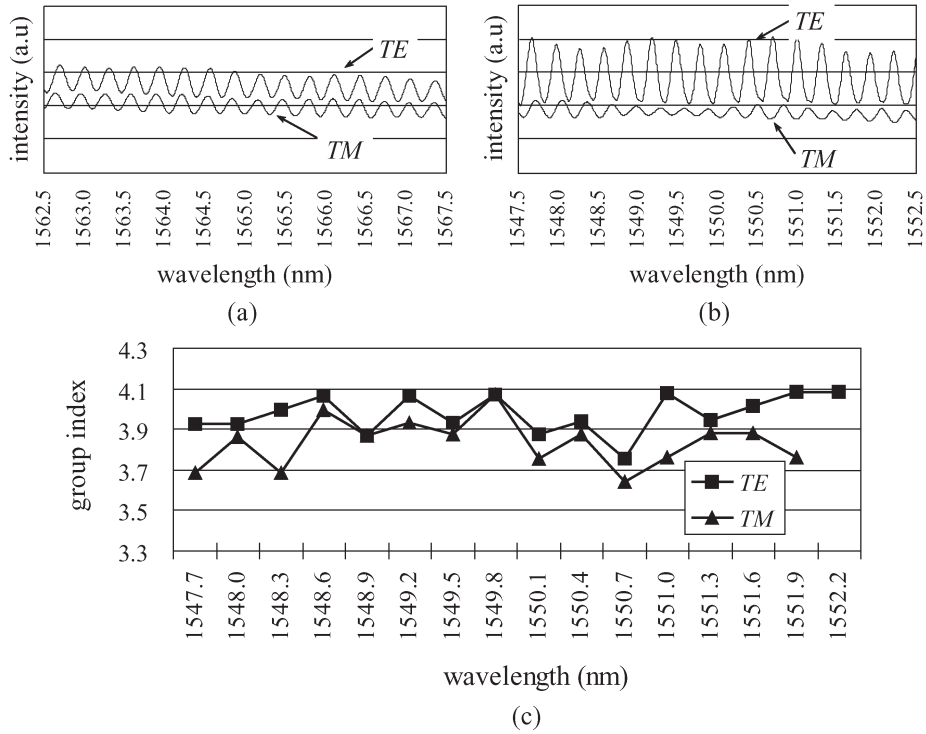


Fig. 1. Polarization resolved ASE spectra for TE and TM polarizations of Kamelian SOA when they are (a) in-phase and (b) out-of-phase. The calculated group index for TE and TM polarizations are shown in (c).

isotropic in the first-order susceptibility. Zinc-blende semiconductors (cubic symmetry class $F\bar{4}3m$, such as GaAs and InP) have a cubic symmetry and are not anisotropic by themselves. However, their third-order susceptibility tensor is intrinsically anisotropic, and they can exhibit strong third-order anisotropy under certain circumstances. The majority of bulk III–V crystals do not feature any birefringence. However, they may become optically anisotropic (birefringent and dichroic) under the action of uniaxial stress [8]. This is the case for bulk materials. In contrast, multiple quantum wells (MQWs) are intrinsically uniaxial due to their layered structure.

Generally, SOAs are polarization sensitive. However, the application of tensile strain in the bulk active region can reduce the polarization dependence. In most cases, the transverse electric (TE) waveguide mode has a higher confinement factor than the transverse magnetic (TM) mode (for the Kamelian SOA in this work, the confinement factors are 0.18 for TE and 0.12 for TM mode), but the tensile strain in the bulk active region makes the TM material gain higher than that of TE. It is therefore possible to balance the two influences leading to polarization independence. This can be expressed as

$$\Gamma_{TE} \frac{dg_{TE}}{dn} = \Gamma_{TM} \frac{dg_{TM}}{dn} \quad (1)$$

where Γ is the confinement factor and (dg/dn) is the rate of change of the optical gain with the carrier density n (differential gain). Therefore, the net gain for TE and TM waveguide mode is equal to each other, meaning that the SOA is polarization independent.

Tensile strain results in an optical anisotropy, and the induced birefringence can be demonstrated by polarization-resolved

amplified spontaneous emission (ASE) spectrum [9]. Fig. 1(a) and (b) demonstrates the spectra at two different wavelengths, and the weak polarization sensitivity of the gain can be used to identify the two orthogonal axes as TE and TM modes of the SOA structure. In the spectra, the small ripples on the curves are due to the residual reflectivities on the SOA facets and show different periodicities for TE and TM polarizations. While both curves are in phase at one wavelength, shown in Fig. 1(a), they may be out of phase at another, shown in Fig. 1(b). By using the general formula of a Fabry–Pérot resonator [10, Ch. 2]

$$\Delta v = \frac{c}{2n_g L} \quad (2)$$

one can determine the group indices for both TE and TM polarizations. Here, Δv is mode spacing, n_g is group index, and L is cavity length. Since the periodicities in the ripple for TE and TM polarizations are not equal, the group velocity index for TE and TM propagations are different. This is depicted in Fig. 1(c). However, a practical challenge of this practice is that the resolution of the spectrum analyzer, typically 0.1 nm, will not be sufficient to fully resolve the peaks and the valleys of the studied modes. Another practical problem is, in the spectrum, the periodicities in the ripple for TE and TM polarizations cannot be obtained precisely enough for one particular mode due to the high sensitivity to the instrument response function and low signal-to-noise ratio (SNR) [11], [12], and no exact dispersion relations are known yet. Therefore, Fig. 1(c) can only demonstrate the general group index difference, and there are some variations of group index both in TE and TM light propagations due to some experimental uncertainties.

B. Structure-Induced Birefringence

It is well-known that modal birefringence in a slab waveguide cannot be eliminated. The boundary conditions usually result in different propagation constants for the lowest order TE and TM, i.e., a structural birefringence [13]. If the tensile strain is not used to minimize polarization dependence, it is possible to fabricate SOAs of square cross-sectional waveguide, which can also achieve polarization-independent operation. However, this type of design is more susceptible to variances in mesa width and exhibits too large far field divergences that can result in poor coupling efficiency. Fortunately, practical semiconductor waveguides are not slab waveguide, and they are not circular or square in shape either [10, Ch. 5]. By proper selection of the waveguide parameters, the modal birefringence B , defined as the difference between the TE and TM effective indices ($N_{\text{eff,TE}} - N_{\text{eff,TM}}$), can be dramatically reduced [14]. With advanced waveguide designs, and utilizing state-of-the-art epitaxial growth, lithography, and etching technology, structure-induced birefringence can be of minor importance in many applications, and is of less concern in this work. However, it is, as always, preferable to keep this structure-induced birefringence as low as possible.

C. Signal-Induced Anisotropy

It has been demonstrated that optically induced anisotropy is observed even in intrinsically isotropic materials [15]. For zinc-blende materials, the third-order susceptibility tensor is intrinsically anisotropic; therefore, they show strong anisotropy at the presence of a pump light, and the magnitudes of the anisotropy of the induced birefringence and of the induced dichroism also depend on the material orientation.

When a strong pump light is coupled into a bulk SOA, the effective refractive index for TE/TM propagation along the semiconductor waveguide is given by

$$N_{\text{TE}}(n) = N_{\text{TE0}} + \Gamma_{\text{TE}} n \left(\frac{dN_{\text{TE}}}{dn} \right) \quad (3a)$$

$$N_{\text{TM}}(n) = N_{\text{TM0}} + \Gamma_{\text{TM}} n \left(\frac{dN_{\text{TM}}}{dn} \right) \quad (3b)$$

where n is the carrier density, N_0 is the effective refractive index of the waveguide for zero carrier density, and (dN/dn) is the rate of change of the active layer refractive index with the carrier density n (differential refractive index). N_0 is different for the TE/TM mode owing to the TE/TM asymmetry in semiconductor waveguide [13]. Typical value for (dN_{TE}/dn) and (dN_{TM}/dn) in $\text{In}_{1-x}\text{Ga}_x\text{As}_y\text{P}_{1-y}/\text{InP}$ material system is -1.44×10^{-26} and $-1.20 \times 10^{-26} \text{ m}^3$, respectively. The confinement factors of Kamelian SOA in this work are 0.18 for TE and 0.12 for TM mode. For an SOA of 2000 μm cavity length at 1.5 μm , this pump-induced TE/TM index difference is on the order of 2×10^{-4} and is sufficiently high to cause a large TE/TM relative phase shift.

It is necessary to point out that, because of carrier depletion due to stimulated emission, the carrier density alone inside the SOA waveguide is not uniform (n is a function of position z

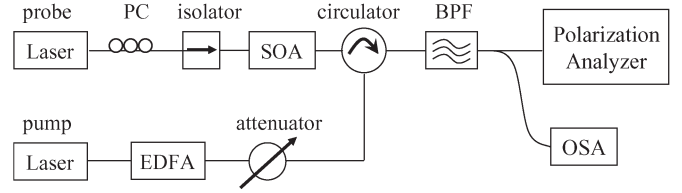


Fig. 2. Experimental setup for the pump-probe geometry in a counterpropagation scheme. PC: polarization controller; OSA: optical spectrum analyzer.

along the cavity length). Therefore, N_{TE} and N_{TM} in (3) not only depend on the carrier density inside the SOA, but also on the position of interest along the cavity length. However, it is beyond the scope of this paper to go into a detailed discussion of this topic, and taking an average of the refractive index of TE/TM mode along the cavity length can still give an insight into this signal-induced birefringence.

Because of the anisotropic nature of zinc-blende structure in the pump-probe scheme, the optical losses experienced by the probe light can also be different for the TE/TM mode, although optical gain is usually assumed equal for TE/TM propagation in a gain-independent SOA. This feature is treated in the next section and presented in the form of Poincaré sphere.

III. PRINCIPLES OF OPERATION

In this work, a pump-probe technique is used to investigate the signal-induced anisotropy of the SOA in a counterpropagation scheme. It is well known that the presence of an intense pump light modifies the optical properties of the SOA which, in turn, modifies a probe light or even the pump light itself [16]. The pump-probe technique that we use in this work is an extension of the Kerr ellipsometry technique [15]. In this procedure, an intense linearly polarized pump light is used to induce a birefringence and a dichroism in the optical properties of the SOA, which are experienced by a weaker probe light. One of the consequences of this optically induced anisotropy in the SOA is that the polarization azimuth and ellipticity angle of the probe are expected to change on the propagation through the medium [17]. The induced azimuth rotation is proportional to the imaginary part of $\chi^{(3)}$ anisotropy, whereas the induced ellipticity change is due to the real part of $\chi^{(3)}$ anisotropy [18, Ch. 7].

This pump and probe geometry is depicted in Fig. 2, and the induced birefringence and dichroism, which lead to a change in polarization azimuth and ellipticity of the probe, are presented in the format of the Poincaré sphere. The SOA is a commercially available pigtailed SOA (Kamelian, OPA series), employing a tensile-strained bulk $\text{InGaAsP}/\text{InP}$ active region. The SOA bias current and temperature are maintained at 200 mA and 20 $^{\circ}\text{C}$, respectively. The wavelength of the probe and pump light is 1558 and 1550 nm, respectively. The polarization analyzer is from Agilent (model: 8509 C), and an HP86142A optical spectrum analyzer (OSA) is used to monitor the output spectrum from the SOA. A bandpass filter (BPF; 1 nm) is placed after the circulator to suppress the spontaneous noise from the SOA. The power of the probe coupled into the SOA is ~ -8 dBm. Since the device anisotropy is rather

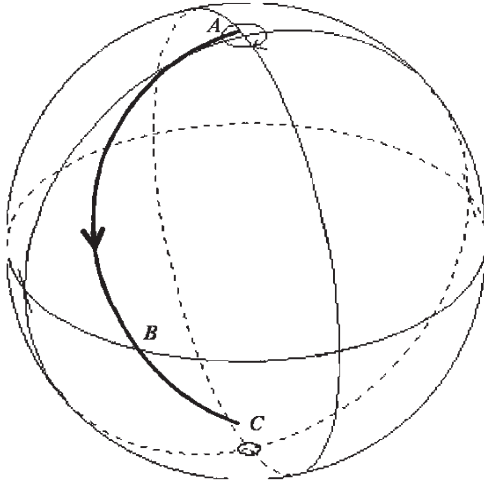


Fig. 3. Solid thick line on the Poincaré sphere indicates how the probe light changes its SOP as the pump light power increases from (A) -6.5 dBm, (B) 5.9 dBm, and (C) 8.0 dBm.

sensitive to the input power level, it is necessary to use a low-power probe light so that the probe does not induce any birefringence or dichroism when acting alone [18, Ch. 4]. Therefore, in the absence of the pump, the state of polarization (SOP) of the probe is preserved, and strong birefringent and dichroic effects owing to the intense pump light dominate inside the SOA.

When the pump light is coupled into the SOA, owing to the TE/TM asymmetry of the confinement factors and carrier distributions, and the induced nonlinear refractive indices and absorption coefficients of the SOA [19], birefringent and dichroic effects are induced. Therefore, the TE and TM components of the transmitted probe experience different phase shifts and different optical gains and losses. As a result, the probe light will change its polarization azimuth and ellipticity to different values, depending on the injected power coupled into the SOA [20]. These changes are presented in Fig. 3, in which the probe light changes its SOP and traces out a thick solid line on the Poincaré sphere as the power of the pump light is varied. At point A on the sphere, with a pump power of -6.5 dBm, the probe is nearly circularly polarized; when the pump power is increased to 5.9 dBm, the probe turns to be linear (point B on the sphere); with further increase of the pump power to 8.0 dBm at point C, the probe is elliptically polarized. It should be noticed that, during this tuning process, not only is the ellipticity angle of the probe changed, but the polarization azimuth is also altered by the optical gain and optical loss mechanism inside the SOA. It can be easily verified from Fig. 3 that, unless the locus ABC followed a longitudinal great circle, the polarization azimuth is different for each point on the locus [21].

A detailed analysis of this optically induced anisotropy in the SOA can be presented by the Stokes–Mueller description. Physically, the SOA can be treated as a polarization element that alters the polarization state of the probe light by changing the amplitude and the phase of its electric-field vector. Since optical gain/loss in the SOA is different for TE/TM propagation, the amplitudes of the electric-field vector of the TE/TM mode of the probe are changed by different amounts. In this sense, the SOA works as a diattenuator. Meanwhile, the TE/TM mode of the probe experiences different refractive indexes, as discussed in Section II, which results in different phase shifts upon leaving the SOA. In this case, the SOA behaves as a phase shifter. In a simplified but physically useful picture, the SOA can be considered simultaneously as a diattenuator and a phase shifter, and this behavior can be described by a Mueller matrix [22], which is originally constructed for an anisotropic absorbing retarder in (4), shown at the bottom of the page.

For convenience, we have used TE and TM orientation of the SOA configuration as the reference axes. Here, $G_{\text{TE/TM}}$ is single-pass gain for TE/TM mode of the probe and is given by [10, Ch. 11]

$$G_{\text{TE/TM}} = \exp [(\Gamma_{\text{TE/TM}} g_{\text{TE/TM}} - \alpha_{\text{TE/TM}}) L] \quad (5)$$

where g and α are the optical gain coefficient and absorption coefficient, respectively. $\Delta\varphi$ represents the additional phase shift between the TM and TE components of the probe due to the existence of the pump light. $\Delta\varphi$ is given by

$$\begin{aligned} \Delta\varphi &= \frac{2\pi L}{\lambda_p} \left[(N_{\text{TM}} - N_{\text{TE}})_{\text{pump_on}} - (N_{\text{TM}} - N_{\text{TE}})_{\text{pump_off}} \right] \\ &= (\varphi_{\text{TM}} - \varphi_{\text{TE}})_{\text{pump_on}} - (\varphi_{\text{TM}} - \varphi_{\text{TE}})_{\text{pump_off}} \quad (6) \end{aligned}$$

and [19]

$$\begin{aligned} \varphi_{\text{TM/TE}} &= \frac{2\pi L}{\lambda_p} \left(N_{\text{TM/TE}} + \Gamma_{\text{TM/TE}} n_p \frac{dN_{\text{TM/TE}}}{dn} \right) \\ &\quad + \frac{2\pi L \Gamma_{\text{TM/TE}} (n - n_0)}{\lambda_p} \frac{dN_{\text{TM/TE}}}{dn} \quad (7) \end{aligned}$$

where λ_p is the wavelength of the probe light, $N_{\text{TM/TE}}$ is the TM/TE effective refractive index averaged along the SOA, $\Gamma_{\text{TM/TE}}$ is the confinement factor at the TM/TE orientation, n_p is the value of the carrier concentration for zero input power at the bias current used to define the peak gain wavelength, n_0 is the transparency carrier concentration, and (dN/dn) is the differential refractive index. A detailed modeling of this signal-induced anisotropy in the SOA is beyond the scope of this paper and will be presented elsewhere. However, some experimental

$$M = \frac{1}{2} \begin{pmatrix} G_{\text{TE}}^2 + G_{\text{TM}}^2 & G_{\text{TE}}^2 - G_{\text{TM}}^2 & 0 & 0 \\ G_{\text{TE}}^2 - G_{\text{TM}}^2 & G_{\text{TE}}^2 + G_{\text{TM}}^2 & 0 & 0 \\ 0 & 0 & 2G_{\text{TE}}G_{\text{TM}} \cos \Delta\varphi & 2G_{\text{TE}}G_{\text{TM}} \sin \Delta\varphi \\ 0 & 0 & -2G_{\text{TE}}G_{\text{TM}} \sin \Delta\varphi & 2G_{\text{TE}}G_{\text{TM}} \cos \Delta\varphi \end{pmatrix} \quad (4)$$

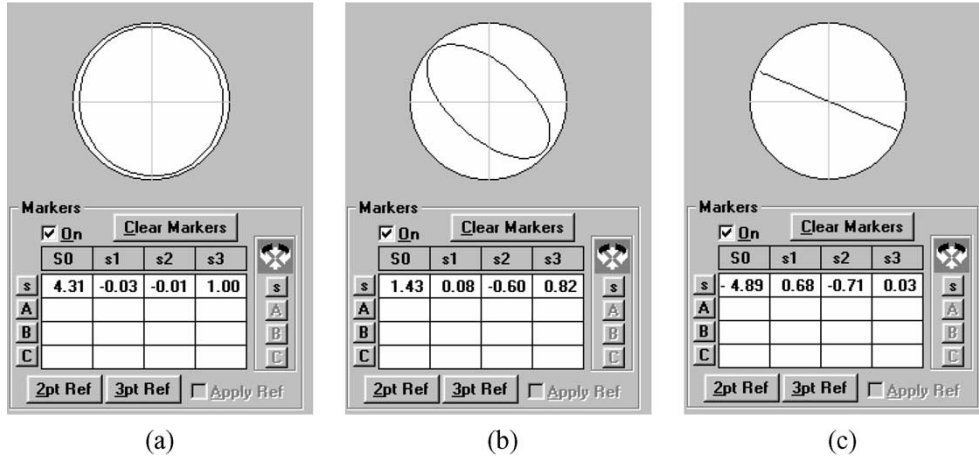


Fig. 4. SOP of the transmitted probe light at different pump light powers. (a) Absence of pump light. (b) -2.8 dBm. (c) 5.9 dBm.

results that are directly related to wavelength conversion are reported here.

Fig. 4 shows how the probe changes its SOP as the pump power increases. Before entering the SOA, the SOP of the probe light is adjusted by a polarization controller (PC in Fig. 2), which makes the SOP of the probe leave the SOA nearly circularly polarized [see Fig. 4(a)] when there is no pump light. When a pump light is coupled into the SOA through an optical coupler and the pump power increases gradually, birefringent and dichroic effects are induced in the SOA and the circularly polarized probe light will change its SOP to be elliptical [with a pump power of -2.8 dBm, shown in Fig. 4(b)] and linear [with a pump power of 5.9 dBm, shown in Fig. 4(c)]. A figure of merit of using the Poincaré sphere to display the change of polarization azimuth and ellipticity angle is that, as the tuning process is visually guided by a moving polarization trace on the sphere, the Stokes parameters are also given for numerical calculations at the same time. Given the Stokes parameters $S(S_0, S_1, S_2, S_3)$ of the incoming probe light and $S'(S'_0, S'_1, S'_2, S'_3)$ of the transmitted probe light upon leaving the SOA, the two Stokes vectors are related by the Mueller matrix, which is defined in (4)

$$S' = MS. \quad (8)$$

In general, even though the incoming probe light is linearly polarized, the existence of the m_{33} term in (4) shows that the polarization of the transmitted probe light will be elliptically polarized. The polarization azimuth θ and the ellipticity angle ε are determined by [18, p. 41]

$$\tan 2\theta = \frac{S_2}{S_1} \quad (9)$$

and

$$\sin 2\varepsilon = \frac{S_3}{S_0}. \quad (10)$$

In Fig. 4(a), the initial polarization azimuth of the nearly circularly polarized probe is 9.2° ; and it changes to -41.2° as the pump power increases to -2.8 dBm in Fig. 4(b). Eventually, when the probe is linearly polarized with a pump power of

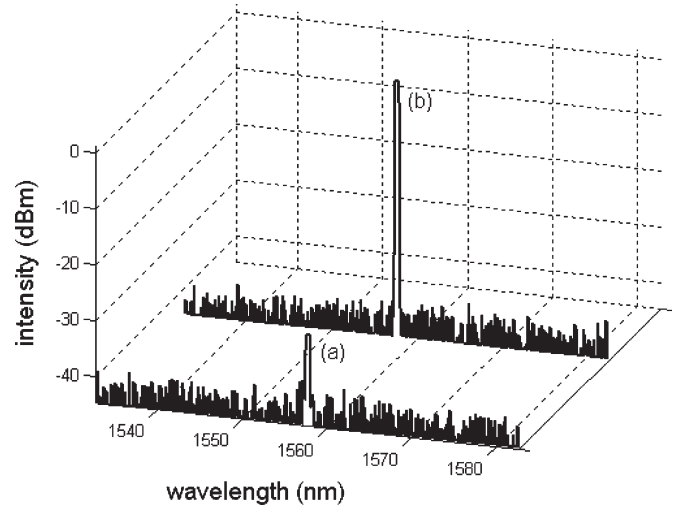


Fig. 5. Optical spectra of the transmitted probe obtained at the output of the polarizer with (a) absence and (b) presence of the pump light in the SOA.

5.9 dBm, shown in Fig. 4(c), the polarization azimuth of the probe is -23.1° . This also confirms our early statement that, in the pump-probe geometry using SOA as the nonlinear medium, not only the ellipticity angle, but also the polarization azimuth of the probe, is changed as a function of pump power.

IV. WAVELENGTH CONVERSIONS BY XPolM

One promising application of this nonlinear phenomenon in SOAs is all-optical wavelength conversions, both inverted/noninverted and upconversion/downconversion. As discussed above, the presence of an intense pump light can induce anisotropy in the optical properties of the SOA, which may be detected by a transmitted probe light. Therefore, when a polarizer is placed after the SOA (the polarizer was actually placed after BPF during the measurements and is not shown in Fig. 2), the phase difference between the probe's TE and TM components can be converted to intensity difference, and wavelength conversion can be realized. Fig. 5 shows the static wavelength conversion by XPolM for the noninverted case. From an application point of view, the noninverted wavelength conversion is always preferred. Spectrum (a) in Fig. 5 is recorded when

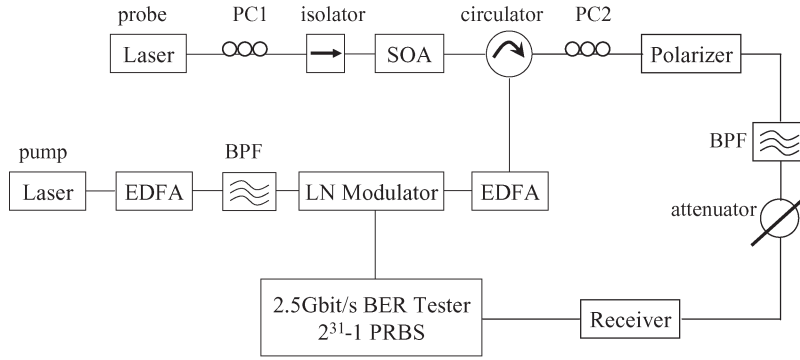


Fig. 6. Experimental setup for all-optical wavelength conversion by XPolM.

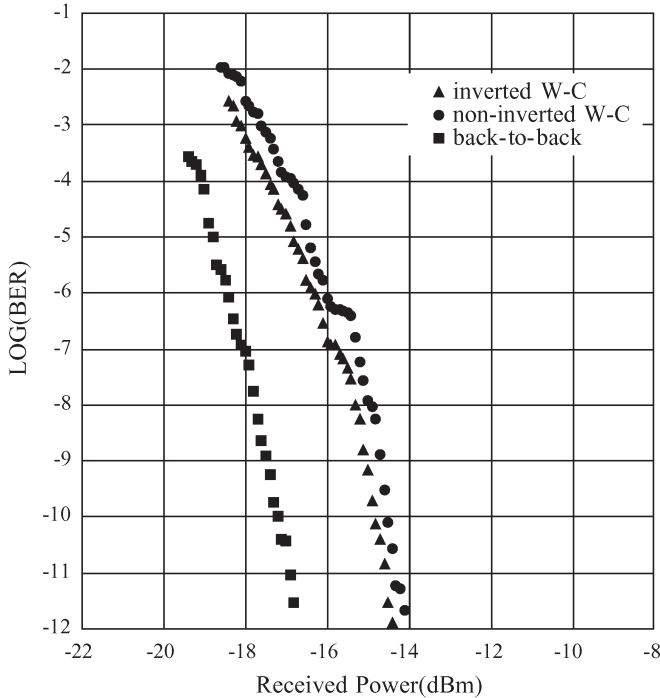


Fig. 7. Plot of 2.488 Gb/s BER measurements for inverted and noninverted wavelength conversions, together with back-to-back measurement. W-C: wavelength conversion.

there is no pump light, and spectrum (b) is obtained when an intense pump light is coupled into the SOA. The ON/OFF ratio is > 30 dB.

The setup for dynamic wavelength conversions using XPolM is depicted in Fig. 6. The pump light is modulated at a bit rate of 2.488 Gb/s with non-return-to-zero (NRZ) pseudorandom bit sequence (PRBS) of length $2^{31} - 1$ via a LiNbO₃ Mach-Zehnder modulator. A BPF (1 nm) is placed after the polarizer to sufficiently suppress the spontaneous noise from the SOA. The SOP of the probe is adjusted by a polarization controller (PC1 in Fig. 6), which ensures its SOP orientation to be set at some angle to the TE (or TM) axis of the SOA. The wavelength of the probe and the pump is 1558 and 1550 nm, respectively; and the power of the probe and the pump light coupled into the SOA is -8 and 8 dBm, respectively.

To demonstrate the high-speed operation of this wavelength converter, bit-error-rate (BER) measurements are performed at 2.488 Gb/s. Fig. 7 shows BER measurements of inverted

and noninverted wavelength conversions, together with back-to-back measurement. It can be seen in Fig. 7 that the inverted wavelength conversion leads to a penalty of ~ 3.0 dB at a BER of 10^{-9} . Noninverted wavelength conversion leads to an additional 0.6 dB penalty compared with the inverted case. This can be explained that inverted wavelength conversion shows better performance due to positive contribution from XGM, which takes place simultaneously with XPolM in the SOA. No error floor is found up to BER as low as 10^{-12} , which indicates excellent conversion performance. The extinction ratios and power penalties of the converted signals are found to be 3.9–14.5 and 2.3–3.8 dB, respectively.

Initially, when there is no attenuation introduced into the system, the Q factor of the converted signal is 22.83 for the inverted wavelength conversion [Fig. 8(a)] and 15.96 for the non-inverted case [Fig. 8(b)]. The eye diagrams in Fig. 8(c) and (d) are measured under the conditions that BERs are optimized around 10^{-9} after introducing a considerable amount of attenuation into the system. The eye diagram of inverted wavelength conversion presented in Fig. 8(c) shows an extinction ratio of 5.20 and a Q factor of 6.06; and the eye diagram of noninverted conversion is presented in Fig. 8(d), having an extinction ratio of 5.82 and a Q factor of 5.96. The time base of the measurements is 100.0 ps/div. The open eyes suggest that there is good potential to operate at an even higher bit rate.

V. DISCUSSIONS

A. XGM Effect in the Operation by XPolM

In this work, we also notice that, since high-intensity pump light is required to saturate the SOA, XGM takes place simultaneously with XPolM. Therefore, when a linearly polarized probe light is modulated by pump-induced anisotropy inside the SOA, not only is the SOP of the probe changed, but the intensity of the probe is also modulated by XGM. This simultaneous XGM can affect the overall performance of wavelength conversion by XPolM and has different contributions to inverted/noninverted and up/down wavelength conversions.

For inverted/noninverted conversion discussed in Section III, the effects of XGM in XPolM operation can be clearly seen in Fig. 4. In the Poincaré sphere, S_0 stands for the total received power. When there is no pump, or pump power of -2.8 and 5.9 dBm, the received probe power is 4.3, 1.4, and -4.9 dBm, respectively. To fully exploit the coefficient of XGM and XPolM

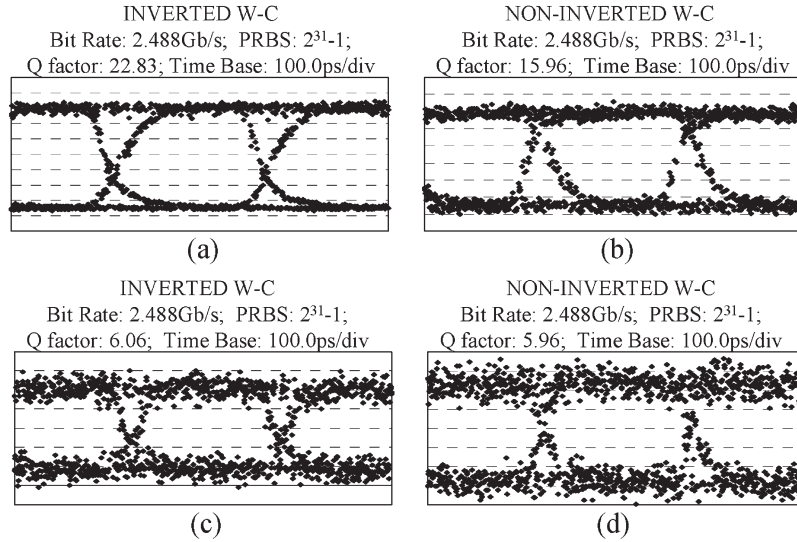


Fig. 8. Eye diagrams for inverted and noninverted wavelength conversions. For measurement details, see the text.

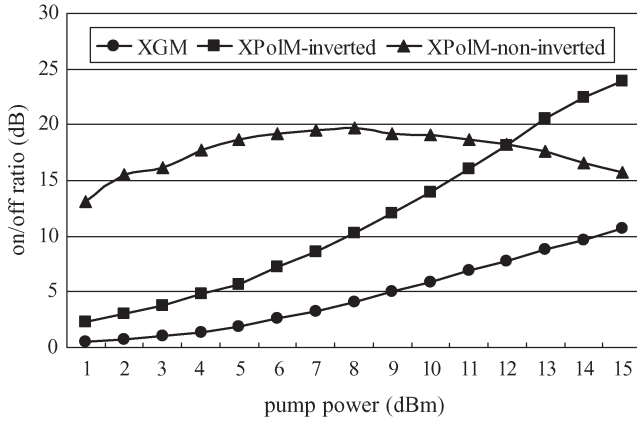


Fig. 9. Comparison of ON/OFF ratio between wavelength conversion by XGM and wavelength conversions by XPolM (inverted and noninverted conversion) as a function of pump light power.

in the converted signals, static modulation by XGM and XPolM with similar setup (both use counterpropagation scheme) were conducted. The experimental results are shown in Fig. 9. For the Kamelian SOA used in this work, the saturation output power is ~ 12 dBm. The ON/OFF ratio of the inverted signal by XPolM is increased, while the ON/OFF ratio of the noninverted signal is decreased when the SOA is being saturated. This can be explained by the fact that XGM enlarges the effect of inverted wavelength conversion but reduces the effect on noninverted case. As a result, the slope of the curve for the inverted conversion is increased and sharper than the one for the noninverted case. This guarantees the better performance of inverted wavelength conversion and explains the reason why noninverted conversion always lead to an additional penalty, as shown in Fig. 7.

In the case of up/down wavelength conversion by XPolM, unlike the discussion above, XGM contributes differently in the operation. As the pump signal reduces the carrier density, the gain of the SOA decreases asymmetrically because of the band-filling effects, as shown in Fig. 10, with the shorter wavelength gain decreasing more rapidly. Because of this asymmetrical

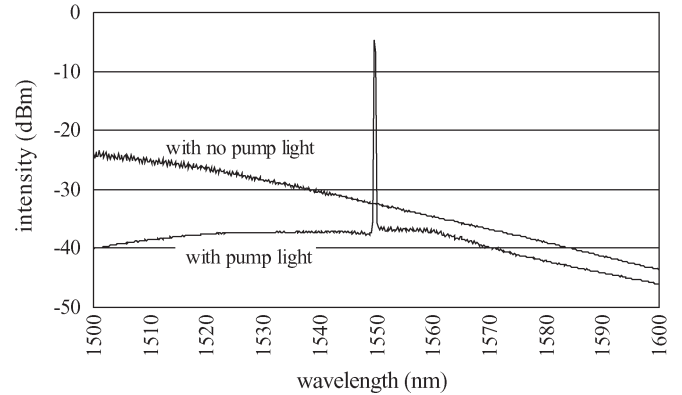


Fig. 10. ASE spectra of Kamelian SOA in the absence and presence of a strong pump light at 1550 nm. The ASE is suppressed more in shorter wavelength than in longer wavelength.

gain compression, the extinction ratio for wavelength conversion by XGM is always better in downconversion. However, for up/down wavelength conversion by XPolM, the larger birefringence induced by the pump light in the longer wavelength range [9] dominates the operation and overcomes the asymmetrical gain suppression effect. This results in a better performance for upconversion. Fig. 11 demonstrates the BER measurement for upconversions/downconversions by XPolM, together with back-to-back measurement. The wavelength of the pump light is 1548 nm, and the probe wavelength for upconversion and downconversion is 1553 and 1543 nm, respectively. The experimental setup is the same as in Fig. 6. It can be seen in Fig. 11 that the upconversion leads to a penalty of 3.2 dB at a BER of 10^{-9} . Downconversion leads to an additional 0.8 dB penalty compared to the upconversion. No error floor is found up to a BER as low as 10^{-12} .

B. Multiple Quantum Well SOA

In this work, we utilize the nonlinearity of a bulk SOA to realize wavelength conversion. However, it is always interesting

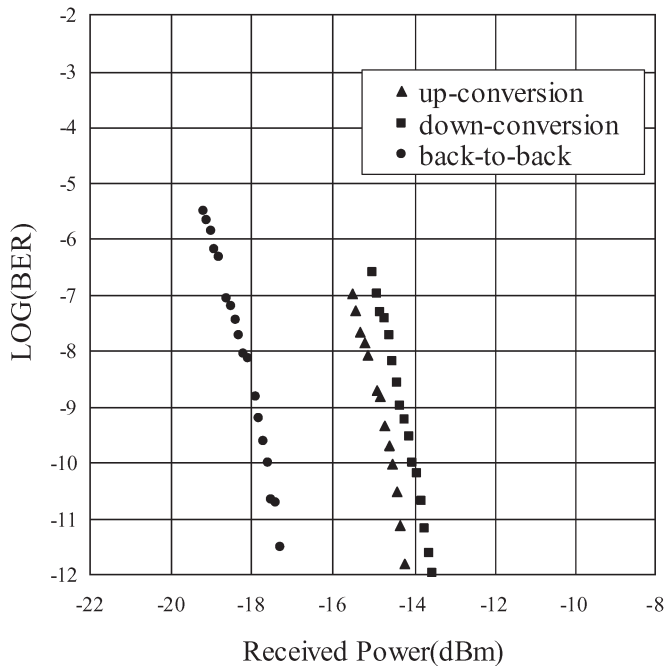


Fig. 11. Plot of 2.488 Gb/s BER measurement for up and down wavelength conversions, together with back-to-back measurement. The wavelength of the pump beam is 1548 nm, and the probe wavelength for upconversion and downconversion is 1553 and 1543 nm, respectively.

to look into wavelength conversion using MQW SOA as the nonlinear medium. Compared with conventional bulk SOA, MQW SOA has many advantages, including high saturation output power, fast gain recovery time [23], and ease of integrability in photonic integrated circuits (PICs). By state-of-the-art well/barrier engineering, MQW SOA with very broad gain bandwidth can also be realized [24]. This is a basic and crucial requirement for large wavelength shift when doing wavelength conversions. Meanwhile, using alternating tensile and compressively strained wells in the active region, polarization-independent gain can be readily achieved [25].

The gain recovery time constant in a MQW SOA can be on the order of 10 ps or less [23], while for non-QW SOA, the gain recovery time is typically 100–300 ps. Because of this rapid gain recovery process, the gain of the MQW amplifier reaches a steady-state more rapidly than does that of a bulk SOA. Meanwhile, due to increased asymmetry of the gain spectrum in QW structure, the differential refractive index (dN/dn) is much enhanced. Previous work showed that (dN/dn) can be as much as 1.8 greater than that of conventional bulk structure [26]. Thus, the optically induced refractive index variation in QW structure is much larger than that of the bulk structure. Both the rapid gain recovery time and the large differential refractive index in QW structure indicate that wavelength conversion by XPolM employing MQW SOA could possibly exceed 40 Gb/s or even higher.

C. Temperature Dependence of (dN/dn)

With decreasing temperature, the variation of refractive index with carrier density increases, as does the variation of optical gain. However, it should be noted that the carrier concentration

also varies with temperature. Thus, the apparent temperature dependence of (dN/dn) will, in general, consist of a pure temperature dependence combined with the effect of carrier density change. A practical issue during the operation of wavelength conversions is the thermal effect caused by the pump light, which will alter the optical properties of the SOA.

VI. CONCLUSION

In this paper, we investigated the signal-induced birefringent and dichroic effects in a tensile-strained bulk semiconductor optical amplifier (SOA) and show that all-optical wavelength conversion by cross polarization modulation (XPolM) is a simple, fast, and robust mechanism. Error-free wavelength conversion at 2.488 Gb/s is obtained. No error floors are observed. Due to the positive contribution from cross gain modulation (XGM) in XPolM, inverted wavelength conversion shows better performance than noninverted case. However, from a practical viewpoint, it is always advantageous for the converted signals to be noninverted.

Although all-optical wavelength conversions in this work were conducted at a bit rate of 2.488 Gb/s, it should be noted that by introducing the enhanced gain recovery technique [27], the data rate could possibly exceed 40 Gb/s. The static coefficient of XGM and XPolM in SOAs is initially studied in the form of ON/OFF ratio. The dynamic effect of XGM in inverted and noninverted wavelength conversions by XPolM is presented in 2.488 Gb/s bit-error-rate (BER) measurements along with back-to-back measurement.

ACKNOWLEDGMENT

L. Q. Guo thanks Dr. Z. Peng and Dr. D. Tong of McMaster University, Hamilton, ON, Canada, for their technical advice and stimulating discussions.

REFERENCES

- [1] S. J. B. Yoo, "Wavelength conversion technologies for WDM network applications," *J. Lightw. Technol.*, vol. 14, no. 6, p. 955, Jun. 1996.
- [2] M. J. Connelly, *Semiconductor Optical Amplifiers*. Boston, MA: Kluwer, 2002, ch. 7, and references therein.
- [3] D. Cotter, R. J. Manning, K. J. Blow, A. D. Ellis, A. E. Kelly, D. Nessel, I. D. Phillips, A. J. Poustie, and D. C. Rogers, "Nonlinear optics for high-speed digital information processing," *Science*, vol. 286, no. 5444, p. 1523, Nov. 1999.
- [4] J. M. Wiesenfeld, B. Glance, J. S. Perion, and A. H. Gnauck, "Wavelength conversion at 10 Gb/s using a semiconductor optical amplifier," *IEEE Photon. Technol. Lett.*, vol. 5, no. 11, p. 1300, Nov. 1993.
- [5] K. L. Hall, E. R. Thoen, and E. P. Ippen, "Nonlinearities in active media," in *Semiconductors and Semimetals*, vol. 59. San Diego, CA: Academic, 1999, p. 83.
- [6] M. F. C. Stephens, M. Asghari, R. V. Penty, and I. H. White, "Demonstration of ultrafast all-optical wavelength conversion utilizing birefringence in semiconductor optical amplifiers," *IEEE Photon. Technol. Lett.*, vol. 9, no. 4, p. 449, Apr. 1997.
- [7] H. Soto, D. Erasme, and G. Guekos, "Cross-polarization modulation in semiconductor optical amplifiers," *IEEE Photon. Technol. Lett.*, vol. 11, no. 8, p. 970, Aug. 1999.
- [8] M. Cardona, "Optical properties and band structure of germanium and zincblende-type semiconductors," in *Atomic Structure and Properties of Solids*, E. Burstein, Ed. New York: Academic, 1972, p. 514.
- [9] S. Diez, C. Schmidt, R. Ludwig, H. G. Weber, P. Doussièr, and T. Ducellier, "Effect of birefringence in a bulk semiconductor optical amplifier on four-wave mixing," *IEEE Photon. Technol. Lett.*, vol. 10, no. 2, p. 212, Feb. 1998.

- [10] G. P. Agrawal and N. K. Dutta, *Semiconductor Lasers*, 2nd ed. New York: Van Nostrand Reinhold, 1993.
- [11] B. W. Hakki and T. L. Paoli, "Gain spectra in GaAs double-heterostructure injection lasers," *J. Appl. Phys.*, vol. 46, no. 3, p. 1299, Mar. 1975.
- [12] D. T. Cassidy, "Technique for measurement of the gain spectra of semiconductor diode lasers," *J. Appl. Phys.*, vol. 56, no. 11, p. 3096, Dec. 1984.
- [13] L. Q. Guo, "Broad-band antireflection coatings for improved grating-external-cavity diode laser performance," M.A.Sc. dissertation, Dept. Eng. Physics, McMaster Univ., Hamilton, ON, Canada, 2002. ch. 2.
- [14] B. M. A. Rahman, S. S. A. Obayya, and H. A. El-Mikati, "Minimization of modal birefringence in semiconductor optical guided-wave devices," *Proc. Inst. Elect. Eng.—Optoelectron.*, vol. 147, no. 3, p. 151, Jun. 2000.
- [15] N. Pfeffer, F. Charra, and J. M. Nunzi, "Phase and frequency resolution of picosecond optical Kerr nonlinearities," *Opt. Lett.*, vol. 16, no. 24, p. 1987, Dec. 1991.
- [16] B. E. A. Saleh and M. C. Teich, *Fundamentals of Photonics*. New York: Wiley, 1991, ch. 19.
- [17] D. C. Hutchings, J. S. Aitchison, and J. M. Arnold, "Nonlinear refractive coupling and vector solitons in anisotropic cubic media," *J. Opt. Soc. Amer. B, Opt. Phys.*, vol. 14, no. 4, p. 869, Apr. 1997.
- [18] Y. P. Svirko and N. I. Zheludev, *Polarization of Light in Nonlinear Optics*. New York: Wiley, 1998.
- [19] M. Asghari, I. H. White, and R. V. Penty, "Wavelength conversion using semiconductor optical amplifiers," *J. Lightw. Technol.*, vol. 15, no. 7, p. 1181, Jul. 1997.
- [20] C. S. Wong and H. K. Tsang, "Polarization-independent wavelength conversion at 10 Gb/s using birefringence switching in a semiconductor optical amplifier," *IEEE Photon. Technol. Lett.*, vol. 15, no. 1, p. 87, Jan. 2003.
- [21] H. G. Jerrard, "Modern description of polarized light: Matrix methods," *Opt. Laser Technol.*, vol. 14, no. 6, p. 309, 1982.
- [22] D. Goldstein, *Polarized Light*, 2nd ed. New York: Marcel Dekker, 2003, ch. 6.
- [23] J. M. Wiesenfeld, A. H. Gnauck, G. Raybon, and U. Koren, "High-speed multiple-quantum-well optical power amplifier," *IEEE Photon. Technol. Lett.*, vol. 4, no. 7, p. 708, Jul. 1992.
- [24] M. J. Hamp, "Asymmetry multiple quantum well lasers," Ph.D. dissertation, Dept. Eng. Physics, McMaster Univ., Hamilton, ON, Canada, 2000.
- [25] M. A. Newkirk, B. I. Miller, U. Koren, M. G. Young, M. Chien, R. M. Jopson, and C. A. Burrus, "1.5 μm multi-quantum-well semiconductor optical amplifier with tensile and compressively strained wells for polarization-independent gain," *IEEE Photon. Technol. Lett.*, vol. 5, no. 4, p. 406, Apr. 1993.
- [26] J. Jacquet, P. Brosseau, A. Olivier, A. Perales, A. Bodere, and D. Leclerc, "Carrier-induced differential refractive index in GaInAsP-GaInAs separate confinement multi-quantum well lasers," *IEEE Photon. Technol. Lett.*, vol. 2, no. 9, p. 620, Sep. 1990.
- [27] R. J. Manning, D. A. O. Davies, D. Cotter, and J. K. Lucek, "Enhanced recovery rates in semiconductor laser amplifiers using optical pumping," *Electron. Lett.*, vol. 30, no. 10, p. 787, May 1994.

Li-Qiang Guo, photograph and biography not available at the time of publication.

Michael J. Connelly (S'89–M'92) was born in Limerick, Ireland, in 1965. He received the B.E. and Ph.D. degrees in electronic engineering from the National University of Ireland, Dublin, in 1987 and 1992, respectively.

He is a Senior Lecturer in Electronic Engineering and Director of the Optical Communications Research Group at the University of Limerick, Limerick, Ireland. His current research interests include semiconductor optical amplifier (SOA) static and dynamic modeling, all-optical signal processing using SOAs, optical coherence tomography, and laser vibrometry.